International Journal of Applied Earth Observation and Geoinformation 40 (2015) 81–90

Contents lists available at ScienceDirect

International Journal of Applied Earth Observation and Geoinformation

journal homepage: www.elsevier.com/locate/jag

Rating health and stability of engineering structures via classification indexes of InSAR Persistent Scatterers

Fabio Pratesi[a,b,*], Deodato Tapete[c], Gloria Terenzi[b], Chiara Del Ventisette[a], Sandro Moretti[a]

[a] University of Florence, Earth Sciences Department, Via La Pira, 4, 50121 Firenze, Italy
[b] University of Florence, Department of Civil and Environmental Engineering, Via di S. Marta, 3, 50139 Firenze, Italy
[c] Durham University, Department of Geography – Institute of Hazard, Risk and Resilience (IHRR) South Road, DH1 3LE, Durham, UK

ARTICLE INFO

Article history:
Received 5 December 2014
Accepted 15 April 2015
Available online 22 April 2015

Keywords:
Structural deformation monitoring
Classification indexes
Synthetic aperture radar
Persistent Scatterer Interferometry

ABSTRACT

We propose a novel set of indexes to classify the information content of Persistent Scatterers (PS) and rate the health of engineering structures at urban to local scale. PS are automatically sampled and grouped via 'control areas' coinciding with the building and its surrounding environment. Density over the 'control areas' and velocity of PS are converted respectively into: Completeness of Information Index (I_{ci}) that reflects the PS coverage grade; and Conservation Criticality Indexes (I_{cc}) which rate the health condition of the monument separately for the object and surrounding control areas. The deformation pattern over the structure is classified as isolated (i) or diffused (d) based on the Velocity Distribution Index (I_{vd}). Both I_{ci} and I_{cc} are rated from A to E classes using a colour-coded system that intentionally emulates an energy-efficiency scale, to encourage the exploitation of PS by stakeholders and end-users in the practise of engineering surveying. Workability and reliability of the classification indexes are demonstrated over the urban heritage of Florence, Italy, using well established ERS-1/2 (1992–2000) descending, ENVISAT (2003–2010) ascending and descending PS datasets. The indexes are designed in perspective of handling outputs from InSAR processing of higher-resolution time series.

1. Introduction

In building surveying, condition assessment is typically provided as a final rate according to a pre-defined scale of lettered or numbered classes (e.g. Salim and Zahari, 2011). Practitioners and end-users find this type of output very effective to express and understand the structural health of the building in a concise, but highly informative way (e.g. Nurul Wahida et al., 2012).

Looking at the current Earth Observation science, Persistent Scatterers (PS) obtained via satellite multi-temporal Interferometric Synthetic Aperture Radar (InSAR) were already demonstrated valuable to monitor engineering structures and historical assets (e.g. Chang and Hanssen, 2014; Giannico et al., 2013; Osmanoğlu et al., 2011; Stramondo et al., 2008). Whereas, from an application point of view, the international relevance of making this technology suitable to support daily practise is proved by the efforts done at various levels to ease the exploitation of PS datasets by stakeholders, for instance in contexts of urban geohazards mapping (e.g. Bateson et al., 2012). Recently indexes were also proposed to automate and simplify the temporal analysis of PS time series (Berti et al., 2013), or to predict PS spatial distribution (Cigna et al., 2014), but not enough attention was paid so far to classify PS properties to generate an output that can be effectively implemented for purposes of building condition assessment.

To fill this gap, in this paper we propose a novel method to transform PS deformation estimates into classification indexes that allow us to rate the health and instability of civil engineering buildings due to structural deformation. We use the 'Index of completeness of information' (I_{ci}) and 'Index of conservation criticality' (I_{cc}) to express the spatial distribution and velocity range, respectively, of the PS covering the building to survey. This means that for each structure we provide a figure of the estimated hazard rate (I_{cc} score, from 'stable structure' to 'critical deformation'), plus the associated level of confidence based on the amount of PS information available over the structure (I_{ci} score, from 'complete information' to 'no data'). These indexes are scored from A to E classes that are colour-coded from green to red to intentionally emulate an energy-efficiency scale, so that the final output of the structural assessment is provided in a format that the users are more familiar with.

* Corresponding author. Tel.: +39 3391574015.
E-mail address: ing.pratesi@gmail.com (F. Pratesi).

http://dx.doi.org/10.1016/j.jag.2015.04.012

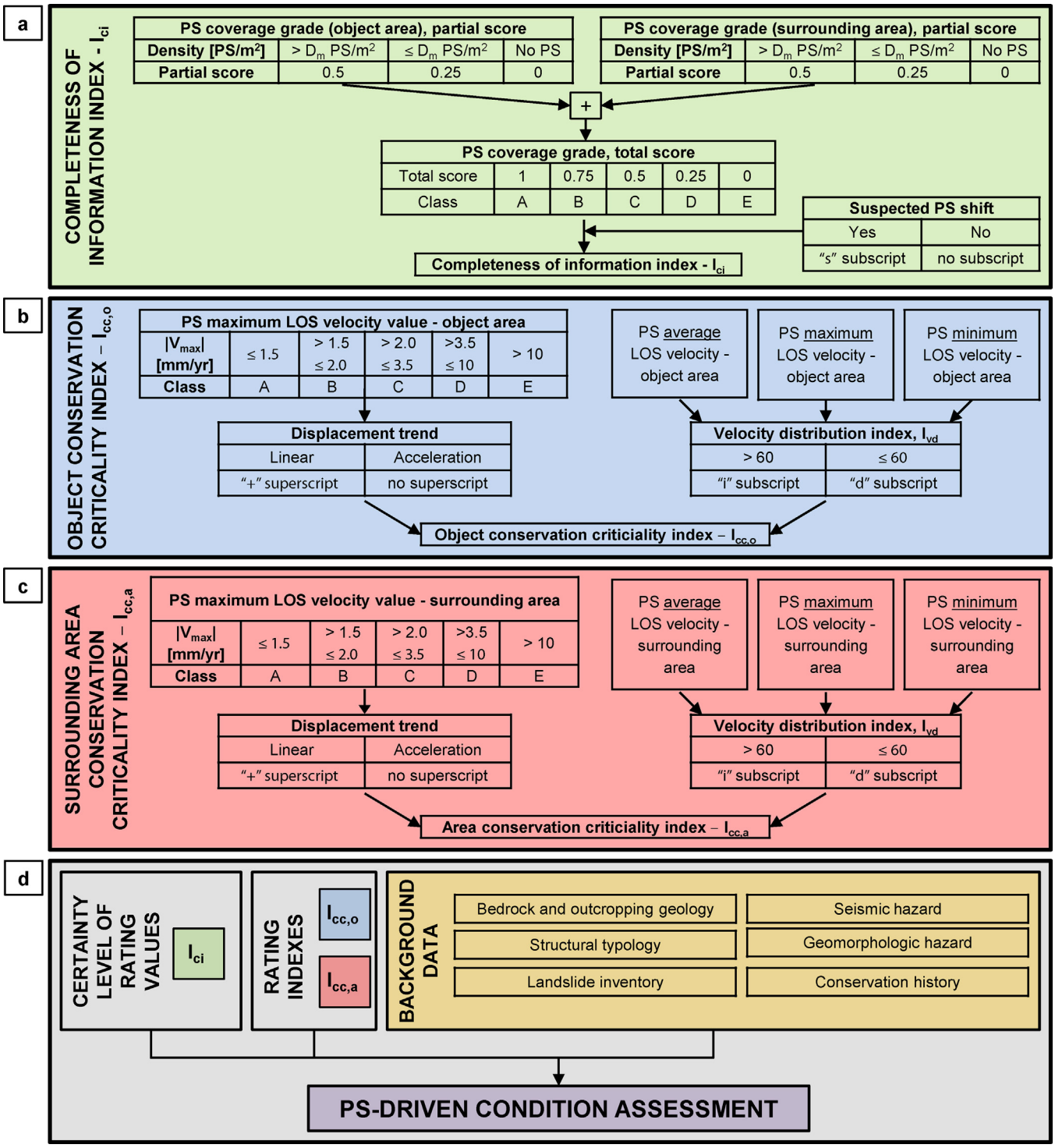

Fig. 1. Procedure of PSI-driven condition assessment for hazard rating of heritage and civil structures, via the calculation of the indexes of: (a) completeness of information (I_{ci}); (b) object conservation criticality ($I_{cc,o}$); (c) surrounding area conservation criticality ($I_{cc,a}$); and (d) final integration of the collected information and indexes (notation: D_m, average PS density).

We apply our method on PS data from ERS-1/2 and ENVISAT ASAR time series covering the built environment of the city of Florence, Italy. We demonstrate that our index-based classification can maximise the PS information of well established datasets also accounting for their intrinsic limitations. The discussion focuses on the novelty that this method can bring into the field of engineering surveying.

2. Methodology

The workflow to classify PS and rate hazard for each structure to survey is reported in Fig. 1. The steps include, in order: the calculation of the 'Completeness of Information Index' (I_{ci}, see Section 2.2), the calculation of the 'Conservation Criticality Index' for the object ($I_{cc,o}$) and for its surrounding area ($I_{cc,a}$; see Section 2.3), and

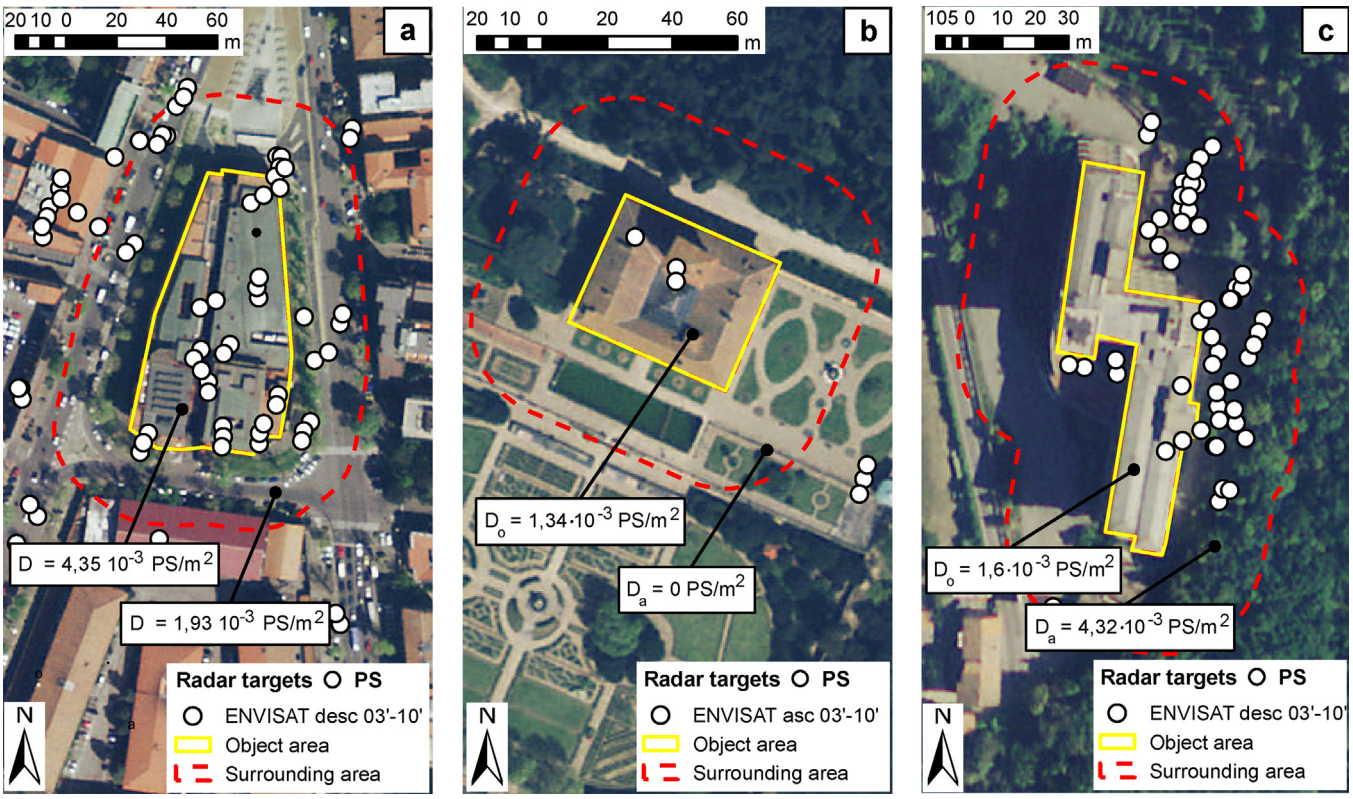

Fig. 2. Example of buildings in the city of Florence with different I_{ci}: (a) National archive – class A, with coverage grade of 0.5 for both the object and surrounding areas; (b) Villa La Petraia – class C, due to 0 PS over the surrounding area; (c) Pratolino sanatorium in the Florentine countryside – class B_s due to the 20 m shift along SW direction for the ENVISAT descending PS dataset.

finally the integration of the collected information and indexes (see Section 3).

2.1. Definition of control area and automatic PS sampling

PS valid for the rating procedure are identified using two distinct control areas (Fig. 2). The object area is drawn exactly along the plan edges of the object derived from cadastral maps and aerial photographs, while the surrounding area is drawn as buffer of the object area the stability of which has impact on the object, with a ray commensurate with the spatial resolution of the SAR images (e.g. 30 m for PS ERS and ENVISAT datasets).

In this way we account for those PS falling outside but very closely to the object boundaries (i.e. in the order of a few metres) that can derive from double-bounce scattering at the corners formed by the object exterior walls and the pavement/ground surface. Keeping these points in the surrounding area helps not to waste informative PS, and counterbalance effects due to the medium resolution of the pixels generating PS during the PSI processing. This is also useful to account for possible non-correct projections of the PS datasets over the geographic support information (e.g. orthophoto, geographic map; cf. Tapete et al., 2015). Furthermore, PS falling within the buffer zone provide displacement estimates that can be retained as meaningful indirect instability indicators for the surrounding field or nearby buildings. These PS, of course, can assume a relevant value in case of objects not covered by PS.

2.2. Completeness of information index – I_{ci}

I_{ci} index numerically expresses how well or bad the object and its surroundings are covered by PS, i.e. the completeness of PS information. The numerical value of this index reflects the density (D) of PS (PS/m^2) falling in the relative control area.

We first calculate the PS density for the object area (D_o). If D_o is 0, less or higher than a fixed threshold of average PS density (D_m), then the partial score attributed takes value of 0, 0.25 or 0.5, respectively (cf. Fig. 1b). PS density for the surrounding area (D_a) is calculated with the same partial score scale as for D_o. I_{ci} is then obtained as sum of D_o and D_a partial scores, so that the final comprehensive I_{ci} is rated from 1 – class A to 0 – class E (with step of 0.25 among two neighbouring classes), i.e. from the highest to the lowest degree of information completeness. Null value of I_{ci} therefore stands for no PS available on both the control areas, and this inhibits the computation of conservation criticality index. No structural assessment and hazard rating is doable, even if PS distributed outside the buffer zone can suggest extrapolation to the study object.

With regard to D_o and D_a calculation, similarly to what discussed by Colesanti and Wasowski, (2006) for rural and low urbanized areas, it is challenging (and, in a sense, also arguable) to use a unique value of average PS density as D_m over urban sites that include a wide spectrum and inhomogeneous distribution of building typologies.

D_m values for the object and surrounding areas are obtained by averaging the values of D_o and D_a found over the full sample of the respective control areas covered by a given PS dataset. For instance, 2×10^{-3} and 1×10^{-3} PS/m^2 were the thresholds to score D_o and D_a, respectively, for the ENVISAT ascending PS dataset, while 1×10^{-3} and 6×10^{-4} PS/m^2 for the corresponding descending dataset (cf. Section 3).

This approach is therefore dataset-specific, and provides a D_m value that best describes the performance of a PSI processing in relation to a given satellite with its own acquisition geometry. This also makes I_{ci} calculation scalable in cases of SAR imagery from very

Table 1
Conservation criticality index (I_{cc}) classes and relative PS velocity range.

I_{cc} Class	Velocity range
A	$\lvert V_{max}\rvert \leq 1.5$ mm/yr
B	1.5 mm/yr < $\lvert V_{max}\rvert \leq 2.0$ mm/yr
C	2.0 mm/yr < $\lvert V_{max}\rvert \leq 3.5$ mm/yr
D	3.5 mm/yr < $\lvert V_{max}\rvert \leq 10$ mm/yr
E	10 mm/yr < $\lvert V_{max}\rvert$

high resolution space missions (e.g. COSMO-SkyMed and TerraSAR-X).

Fig. 2 shows some examples of I_{ci} scoring. Subscript "s" is added to the I_{ci} final rate (e.g. A_s), to indicate that PS are shifted (Fig. 2c).

2.3. *Conservation criticality index* – I_{cc}

This index expresses numerically the condition of the study object and its surroundings based on the maximum value (V_{max}) of the displacement velocity estimated along the Line-Of-Sight (LOS) for the entire monitoring period, among all PS in the relative control areas.

Similarly to I_{ci}, for each PS dataset two separate values of $I_{cc,o}$ and $I_{cc,a}$ are calculated for the object and its surrounding area.

Based on the V_{max} value found in the respective control areas, $I_{cc,o}$ and $I_{cc,a}$ are ranked using a scale of 5 classes of Conservation criticality index. Table 1 reports the scale adopted for the city of Florence, Italy, (cf. Section 3) the lower and upper limits of which are here commensurate with the velocity distribution of the ERS-1/2 and ENVISAT PS datasets.

Velocity intervals are determined based on the radar technical parameters and the statistical distribution of velocity values across the whole PS dataset. The velocity range associated to a stable object (i.e. class A) depends on the single measure precision achievable by the radar technique and then on the radar band frequency. Accounting for the C-band radar sensor used here and the standard deviation of the PS datasets exploited, a velocity threshold of ±1.5 mm/yr is recommended (i.e. class A with $\lvert V_{max}\rvert \leq 1.5$ mm/yr). As well reported in the literature (Hanssen, 2005; Crosetto et al., 2010; Cigna et al., 2013), velocities higher than 15 cm/yr inhibit PSI processing of C-band SAR imagery, and are not easily detected with this technique. In this sense the upper limit of the class E also accounts for the velocity distribution of the PS datasets. The scale reported in Table 1 is tuned to intercept the velocity range which is populated by the majority of the PS measures of the data stack.

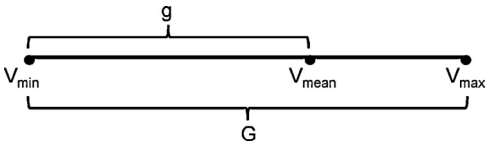

Fig. 3. Conceptual sketch of the LOS velocity variables required to calculate I_{vd}.

2.4. *Velocity distribution index* – I_{vd}

The quantity of unstable PS and their spatial relationship with stable PS in a control area does not modify the value of I_{cc}. To numerically express the distribution of deformation estimates, we introduce the Velocity distribution index (I_{vd}) to be calculated for each control area as follows (Fig. 1b, c and Fig. 3):

$$I_{vd} = (g/G) \times 100$$

where"g" is the maximum value between (V_{max}–V_{mean}) and (V_{mean}–V_{min}) "G" is given by (V_{max} –V_{min}), with "V_{max}", "V_{min}" and "V_{mean}" as the maximum, minimum and arithmetic mean PS LOS velocity valuein the relative control area, respectively.

I_{vd} expresses the symmetry degree of all PS velocity values in a control area with respect to V_{mean} and can be determined if at least 3 PS are available within a control area.

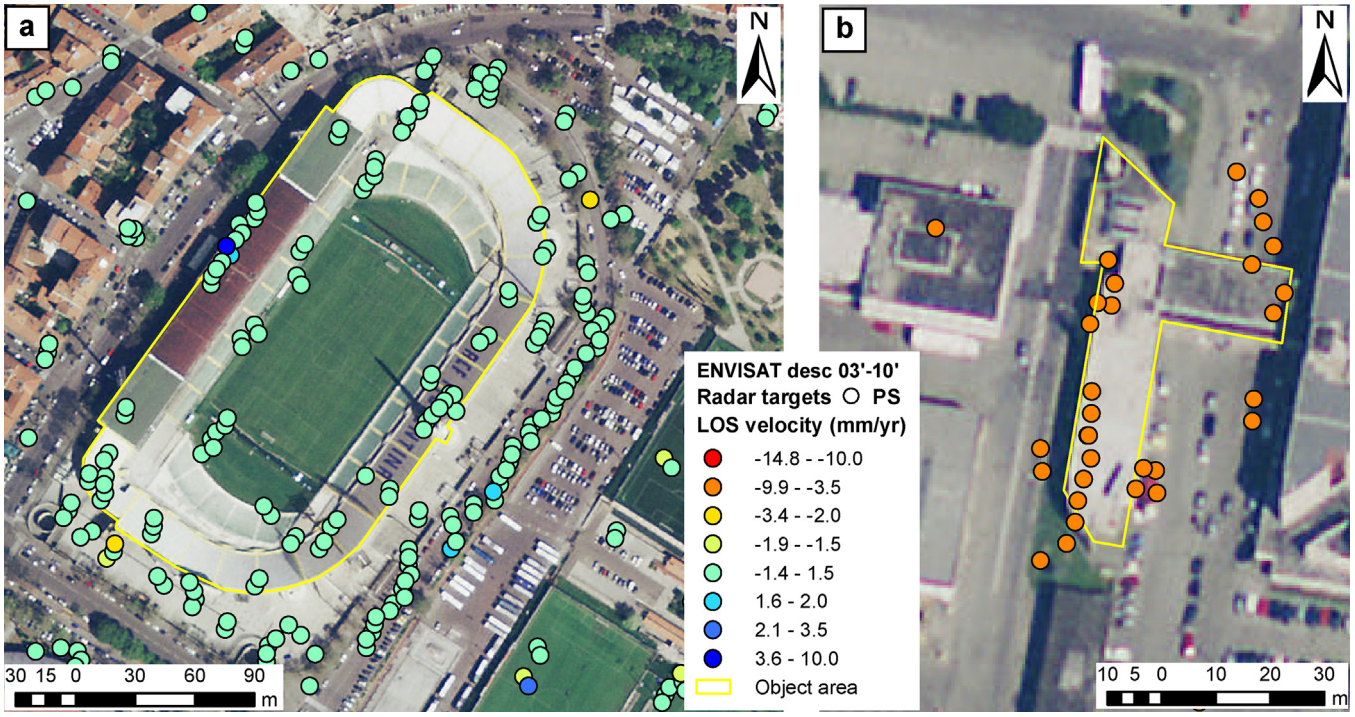

Fig. 4. (a) ENVISAT descending PS 2003–2010 over the Artemio Franchi stadium with I_{vd} value of 76%, which reflects an inhomogeneous velocity distribution, with isolated deformation against an overall stability. (b) Differently, the same dataset over theMERCAFIR commercial area, periphery of Florence, Italy, show a uniform displacement pattern with (V_{max}–V_{mean}) that equals (V_{mean}–V_{min}), thereby leading to I_{vd} value of 51%.

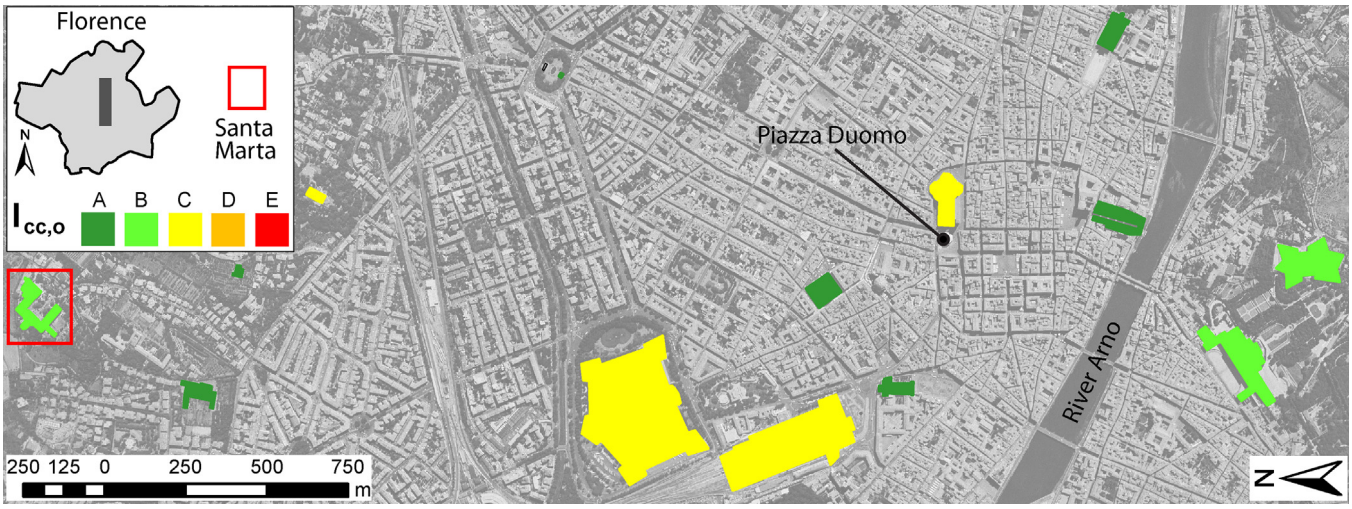

Fig. 5. Distribution of $I_{cc,o}$ indexes over a sector of Florence calculated using ENVISAT ascending data. (For interpretation of the references to colour in the text, the reader is referred to the web version of this article.)

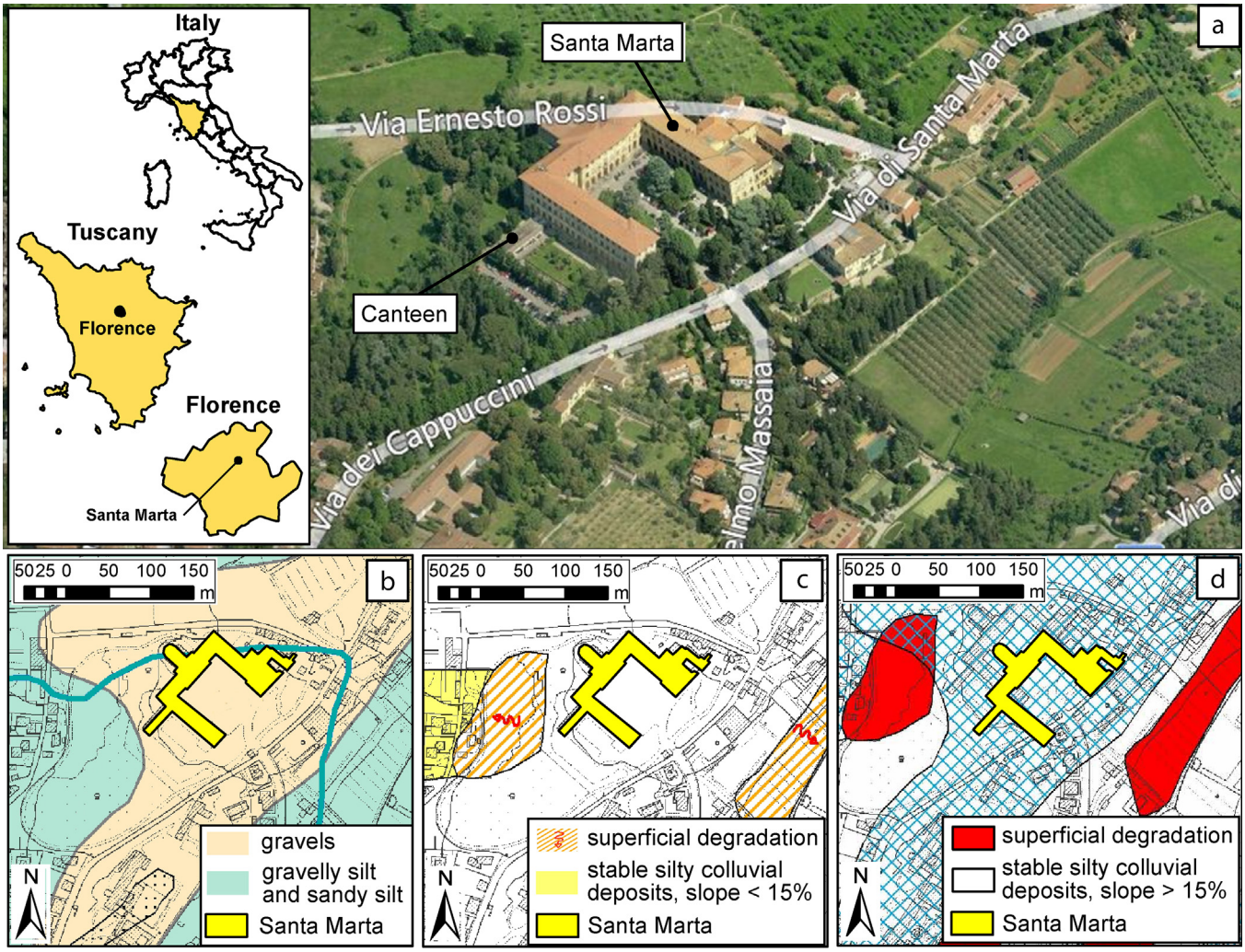

Fig. 6. (a) Aerial view of the monumental building of Santa Marta, Florence, Italy (©BingMaps), and corresponding (b) lithological, (c) hydrogeological hazard and (d) seismic effects maps (modified from Florence City Council, 2010).

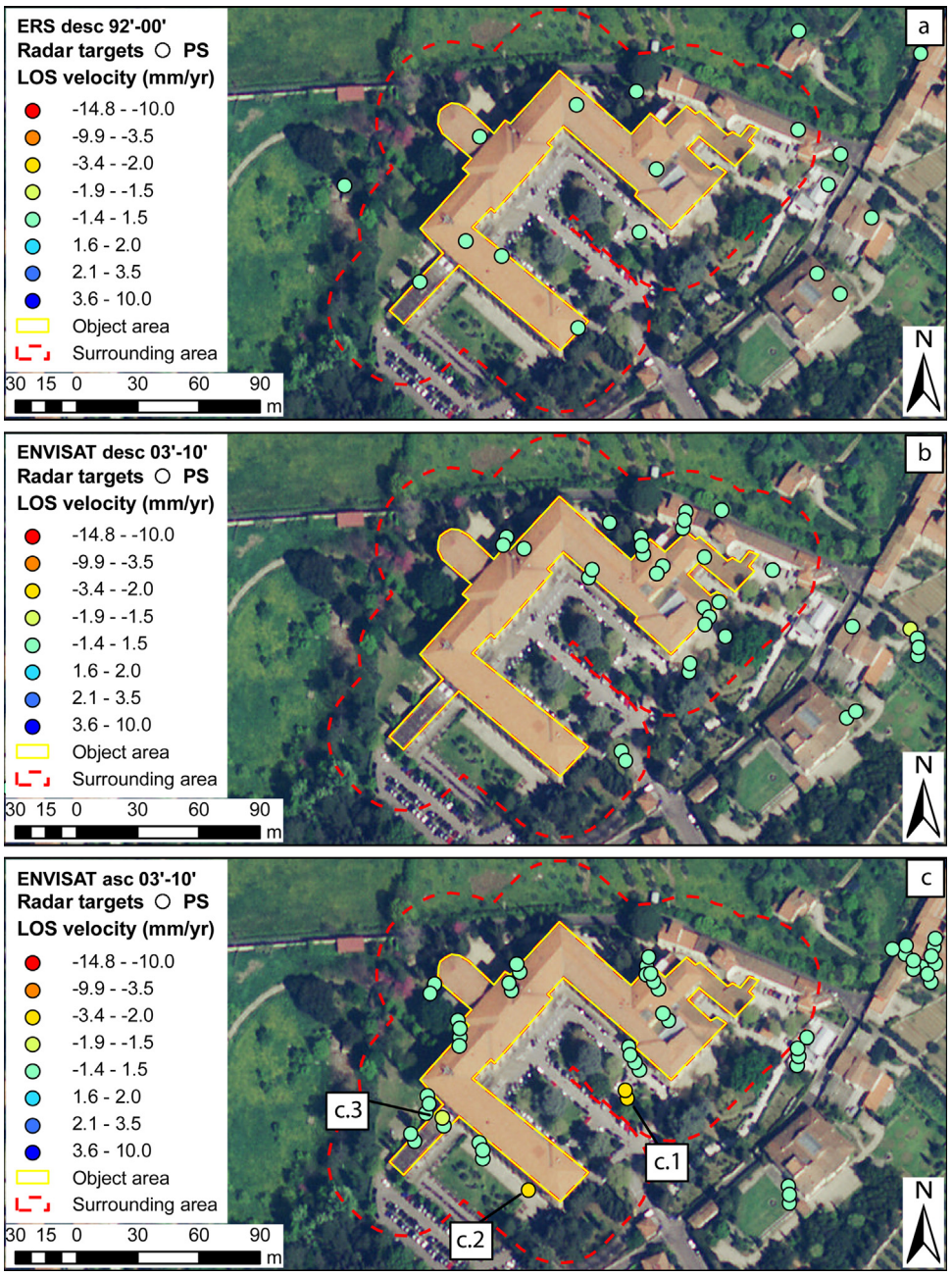

Fig. 7. PS spatial distribution of (a) ERS-1/2 descending 1992–2000, (b) ENVISAT descending 2003–2010, and (c) ENVISAT ascending 2003–2010, over Santa Marta, Florence, Italy. Labels c.1, c.2 and c.3 in picture (c) mark PS that are discussed in Section 3.4 and the time series of which are reported in Fig. 9.

The minimum value that I_{vd} can take is 50% that happens when (V_{max}–V_{mean}) equals (V_{mean}–V_{min}), meaning that the PS velocity distribution is uniform across all the PS falling within the control area (Fig. 4b).

Conversely, higher values of I_{vd} are obtained when the PS velocity interval between V_{mean} and V_{max} is different than the PS velocity interval between V_{mean} and V_{min}, meaning that the PS velocity distribution is not uniform. The latter is the case of a localized deformation usually marked by few single moving PSs in contrast with the majority of stable PSs in the control area. I_{vd} helps to depict this inhomogeneity especially when it is not obvious from the overview of PS spatial distribution (Fig. 4a).

It is recommended that the choice of the I_{vd} threshold to discriminate concentrated deformation from uniform displacement patterns is based on the spatial distribution of the I_{vd} values obtained across the analysed dataset.

Following this approach, the I_{vd} threshold used in Florence equals 60%. If I_{vd} > 60%, the deformation pattern can be considered diffused and a "d" subscript is put next to the class indicator of I_{cc}. If I_{vd} <60%, the detected deformation is considered isolated and "i" subscript is used.

The analysis of PS displacement trend during the last monitoring period, although not explanatory of the present damage, enables the assessment of the evolution state of the ongoing process and forecast of future activities. I_{cc} is then completed adding "+" superscript when displacements estimated with PSI processing technique accelerate, whereas "–" superscript in case of deceleration.

Table 2
Main characteristics of the PSI datasets used to rate hazard of engineering and historical structures in Florence, Italy. PSInSAR processing technique is according to Ferretti et al. (2001).

Data stack	λ[cm]	Orbit	Repeat cycle [days]	Nominal ground resolution [m]	Time interval	No. SAR images	Processing technique
ERS-1/2	5.66	Descending	35	25	24/04/1992 27/11/2000	79	PSInSAR
ENVISAT ASAR	5.63	Ascending	35	30	16/10/2003 27/05/2010	35	PSInSAR
ENVISAT ASAR	5.63	Descending	35	30	10/02/2003 28/06/2010	35	PSInSAR

3. Results and discussion

We applied I_c, I_{cc} and I_{vd} indexes to classify PS from ERS-1/2 and ENVISAT ascending and descending time series over Florence, Italy (Table 2), including the historical city centre, areas of recent urbanization and the hilly surroundings. We purposely implemented a multi-sensor approach, accounting for the variability of PS characteristics. The Florentine test site was selected for its intrinsic variability in terms of characteristics and density of civil structures, morphology and geological properties of the ground.

To have samples of statistical significance, we calculated the classification indexes over different categories of buildings, including: gates and arches (27.3% of the total number in Florence), stadiums (33.3%), convents and churches (29.4%), fortifications (50%) and 20th century architecture (9.5%). With regard to ENVISAT ascending PS coverage, for instance, I_{ci} spatial distribution highlights that more than 20% of the surveyed buildings is scored 'A', while only 12.8% have partial or poor PS coverage (i.e. from 'D' to 'E'). I_{ci} is therefore our measurement of the degree of confidence to rely on the PS falling within the control areas.

Fig. 5 shows the spatial distribution of the $I_{cc,o}$ indexes over the historic centre of Florence, as per classification of ENVISAT ascending PS. Differential condition across the urban area is apparent, and the colour-coding rating system clearly highlights at a small-scale the buildings that require priority attention based on the PS properties.

The benefits that this type classification brings to engineering surveying at single building-scale are discussed with regard to the ex-Episcopal seminary of Santa Marta (see red square in Fig. 5). This building hosting the Faculty of Engineering of the University of Florence serves here as an exemplar to demonstrate the added values and mutual complementary nature of the three classification indexes.

3.1. Background data

The monumental building is located in via de' Cappuccini, at the top of a hill at the northern border of the alluvial plain of the city of Florence (Fig. 5a). In 1980 the University of Florence converted the existing Episcopal seminary to host the faculty offices, library and lecture rooms; additional parts were built in the following years, such as the south-west wing hosting the canteen (Fig. 6a). Apart from the latter, no other significant structural renovation or demolition are recorded.

Actually the building is made of masonry structures, with a C-shape plant (Fig. 6), constant through all the four floors, one of which is partially underground.

The bedrock underneath the building is made of gravels with a fine part of 5%–20%, locally reaching 20–50%. This layer lies upon alluvial deposits of silt and clays dating to late Pleistocene and early Pliocene, the border of which is only 40 m distant to the south-west edge of Santa Marta and 6 m to the south–west edge of the canteen (Florence City Council, 2010) (Fig. 6b).

In correspondence with this discontinuity, the hydrogeological risk map provided by the Florentine City Council marks an area of superficial degradation due to lack of maintenance of drainage systems (Fig. 6c). This area corresponds with the west sector of a more extended paleo-landslide of colluvial silty deposits that is classified as stable. The same area is indicated on the Council map of seismic effects as prone to instability in case of earthquakes (Fig. 6d). However, the official landslide inventories do not report active or dormant landslides that already affect the building or its annexes directly.

3.2. Completeness of information

Starting from the older dataset, I_{ci} of the ERS-1/2 descending PS is rated B which is consistent with the fact that all portions of the building are covered by PS, although their density is quite low, i.e. 10^{-3} PS/m^2 (Fig. 7a).

Conversely, the ENVISAT descending dataset covers only the north-eastern half of Santa Marta (Fig. 7b), thereby resulting in incomplete information for a considerable portion of the building, i.e. in this case the portion closer to the area mapped as prone to instability and where structures of different periods and structural properties intermingle. The major consequence is that only a partial condition assessment is doable, with low degree of certainty and confidence. This concept is clearly summarized by C class for I_{ci} that reflects D_o and D_a values 10^{-3} PS/m^2 and 8×10^{-4} PS/m^{2}of PS densities.

On a comparative scale, the best I_{ci} equal to A_s is obtained for the ENVISAT ascending dataset (Fig. 7c and Table 3), which provides higher density of PS covering the whole building, i.e. 2×10^{-3} PS/m^2. A good density of PS also eases the identification of suspected shifts, in this case inferred from the PS misalignment along the south–west edge of the building.

3.3. Conservation criticalities

Both $I_{cc,o}$ and $I_{cc,a}$ for the ERS-1/2 descending data are rated A (see Table 3). This is consistent with the general stability revealed by all PS for the 1992–2000 period, as well as with the absence of ground instability phenomena mapped on the building area in the official mapping documents.

Differently, with regard to the ENVISAT ascending dataset, rates for $I_{cc,o}$ and $I_{cc,a}$ are B_i and C_i, respectively. The latter, in particular, reflects the effect due to four PS the LOS velocity value of which exceeds the stability threshold of 1.5 mm/yr (Fig. 7c, PS labelled as c.1, c.2 and c.3). These points are localized in three different sectors of the building, while the remaining parts PS do not indicate movement. The presence of a localised deformation pattern is effectively pointed out by I_{vd} values of 70.74% for the object area and 66 % for the surrounding area. Furthermore, the image reported in the Evaluation form reveals that two PS (i.e. "c.2" and "c.3" in Fig. 7c) are located on the south-west edge of the building not far from the area mapped as prone to instability.

Table 3
I_{ci}, $I_{cc,o}$ and $I_{cc,a}$ for Santa Marta, Florence, Italy.

Data stack	I_{ci}	$I_{cc,o}$	$I_{cc,a}$
ERS desc	B	A_i	A_d
ENVISAT desc	C	A_i	A_d
ENVISAT asc	A_s	B_i	C_i

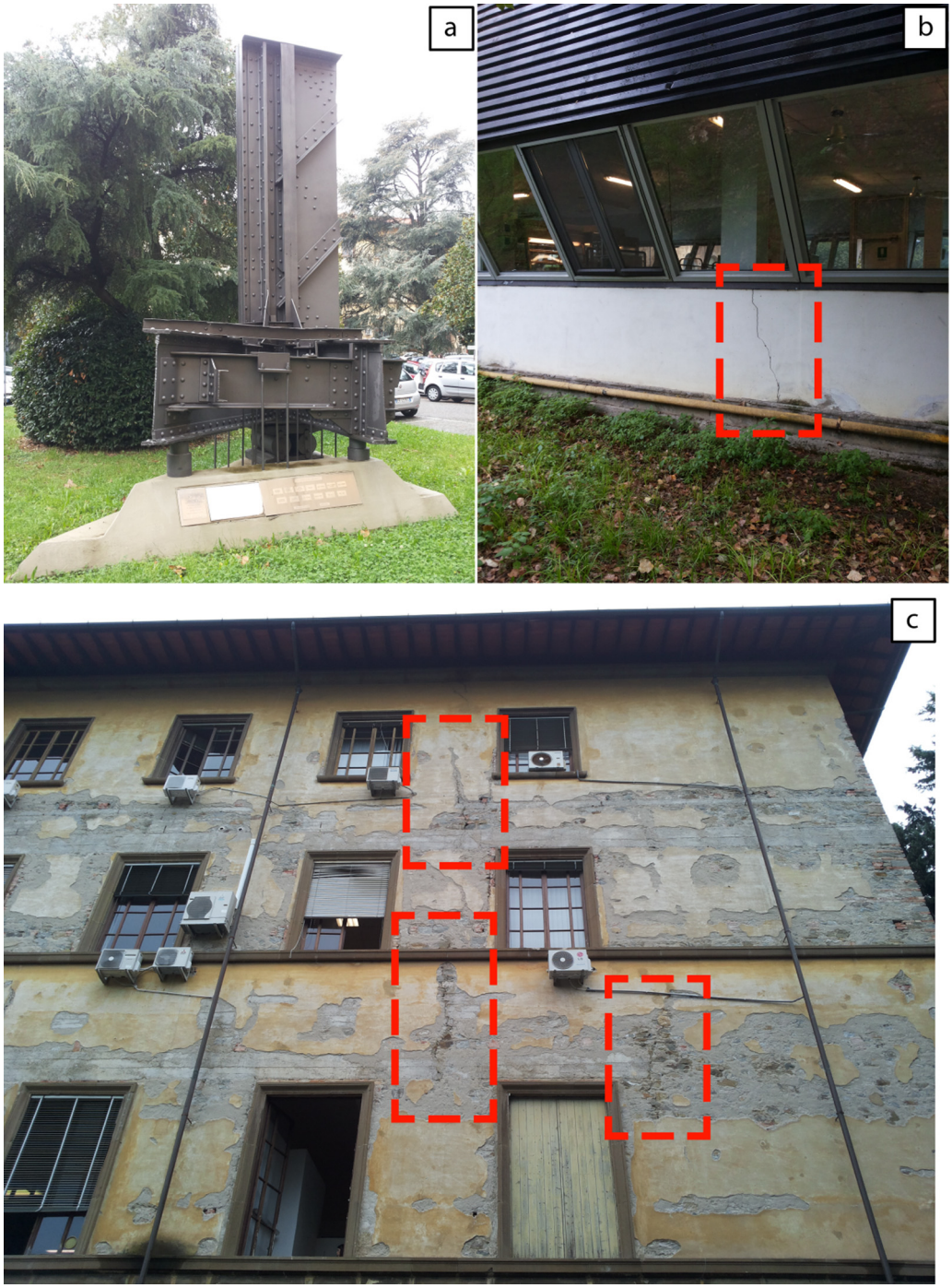

Fig. 8. (a) Contemporary sculpture installation, (b) façade of the canteen annexe and (c) the western façade of the main building of Santa Marta (photographs taken in October 2014) for which the ENVISAT ascending PS 2003–2009 show instability. Dotted red boxes in (b) and (c) mark major fissures running across the masonry and concrete structures. (For interpretation of the references to colour in this figure legend, the reader is referred to the web version of this article.)

3.4. Ground-truth validation

Based on the evidence collected during an on-site validation survey, the ENVISAT ascending PS labelled as c.2 (Fig. 7c) were found to fall in correspondence to a portion of the south-west façade of the building that is severely affected by vertical fractures. One of the latter in particular runs through the 2nd floor level (Fig. 8c). Although all the façades of the complex reveal lack of maintenance, this is the only portion where fissures deepen into the fabric. Therefore, we cannot exclude that the former connections between the structural elements were locally damaged. On the other side, it is certain that movements have occurred with a deformation trend away from the satellite (V_{mean} of −2.9 mm/yr) from 2003 to 2010, as recorded in the PS time series (Fig. 8b). It is important to observe that the approach of counting PS in the buffer area prevented the loss of this PS that, otherwise, would have been not taken into proper account (cf. Section 2.2).

The PS labelled c.3 is spatially attributed to the north-west side of the canteen wing (Fig. 7c). Here a sub-vertical fracture is visible (Fig. 8b). Although the PS V_{mean} equals to −1.6 mm/yr, the abrupt discontinuity observed in the time series of LOS displacements in the course of year 2008 is not

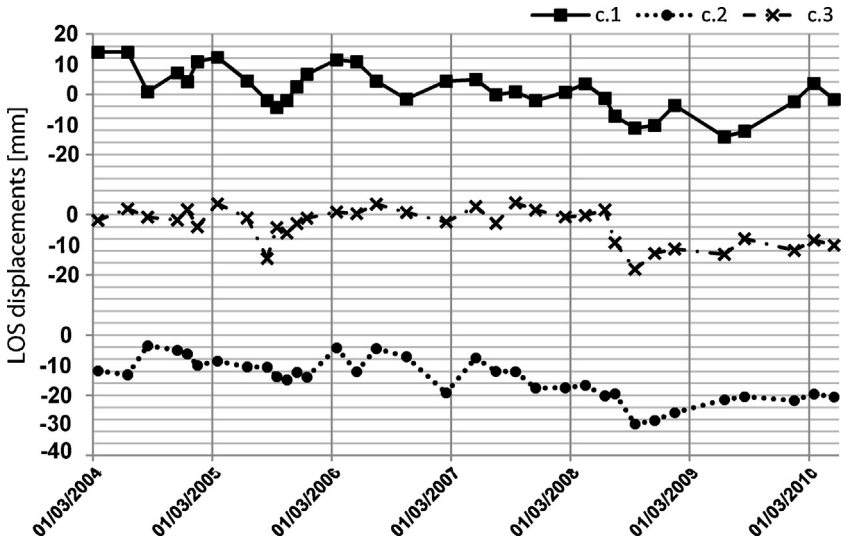

Fig. 9. LOS displacement time series for the PS labelled c.1, c.2 and c.3 in Fig. 7c identified over Santa Marta, positioned over the building portions and sculpture reported in Fig. 8. Negative values stand for movements away from the sensor, positive values stand for movements towards the sensor. Average LOS velocity equals −2.4 mm/yr, −2.9 mm/yr and −1.6 mm/yr, respectively.

negligible (Fig. 9 c.3). We cannot exclude that this is a sign of a failure occurred at that time.

The two PS labelled as c.1 (Fig. 7c) fall over an isolated 4 m-high steel monument (Fig. 8a), that was installed at the end of October 1993. The presence of a high reflecting element in a vegetated context generates an unrelated PS that provides measurements of objects without physical interaction with the analysed structure. In fact, displacements measured for these PS are likely attributed to a settling of the foundation ground of the monument, rather than to a generalised instability of the neighbour area that is not confirmed by other moving PS. This interpretation is also supported by the clear seasonality observed within the LOS displacement trend away from the satellite throughout the time series (Fig. 9 c.1), which is compatible with natural response of the soil surrounding the monument. This case also well clarifies the importance of keeping separate $I_{cc,o}$ and $I_{cc,a}$. Once the PS is found to be not pertinent to the building, $I_{cc,a}$ value should be updated by removing from the count all the unrelated PS from the surrounding area. In such circumstance, the updated value of $I_{cc,a}$ is still rated C_i as the maximum PS velocity value in the surrounding area belongs to the PS labelled as c.2 while the I_{vd} value increases from 66% to 75.5%.

4. Conclusions

The hazard rating procedure proposed in this paper helps to make the best out of the density, spatial distribution and velocity information offered by PS datasets, by converting them into an output that surveyors and end-users can be familiar with and easily understand, i.e. colour-coded rates. In doing so, the procedure accounts for the advantages, but also the shortcomings typically associated with the PS coverages. In this sense, the introduction of I_{ci} index allows us to numerically account for the actual coverage, and therefore unequivocally states if the performed condition assessment is sound and relevant.

The demonstration over the urban heritage of Florence proves the suitability of the colour-coding rating system. Surveyors can identify clearly, even at small scale, the buildings that require attention and further investigation.

The methodological flow to calculate the classification indexes was purposely trained on three PS dataset from PSInSAR processing of medium-resolution C-band imagery, i.e. well established SAR time series and InSAR processing techniques that still are among the longest SAR archives currently available for real-world applications and a precious source of historical information for scientists and practitioners. The copious number of SAR images constituting the time series is an essential requisite to rely on the LOS velocity values and displacement trends observed in the time series.

The above properties justify the use of this satellite data, although it is arguable that the spatial resolution of archive imagery is not ideal anymore in light of the developing catalogues of high resolution SAR imagery acquired by the second generation spaceborne radar sensors (e.g. those onboard TerraSAR-X and COSMO-SkyMed operating in X-band, and the recently launched Sentinel-1A imaging in the C-band).

In this changing scenario of satellite missions, the added value of this procedure lies on its flexibility to adapt to the PS dataset, the properties of the satellite and the site-specific performance over a given study area. Flexibility practically means that the score and class rating system is open to be adjusted to account for: (i) higher PS density as expected outputs from PSI processing of high resolution SAR imagery by means of processing algorithms aiming to increase the numbers of measurement points; (ii) different ranges of LOS velocities.

Further advance of this research is the ongoing testing of the procedure on higher resolution data, with shorter repeat cycle, processed with different algorithms. The demonstration over Santa Marta in Florence, on the other side, is a proof of concept of the current exploitation of this procedure for engineering surveying to assess safety of public fabric and buildings.

Acknowledgments

This research, founded by PRIN PROJECT 2010–2011 Time-space prediction of high impact landslides under changing precipitation regimes, was led by F. Pratesi who designed the rating procedure and carried out the geospatial analysis with the contribution of D. Tapete. PS datasets used were accessed via the WMS service of the National Geoportal of the Italian Ministry of Environment, Territory and Sea.

References

Bateson, L., Cuevas, M., Crosetto, M., Cigna, F., Schijf, M., Evans, H., 2012. PANGEO: enabling access to geological information in support of GMES: deliverable 3.5

production manual. Version 1. Available at: </http://www.pangeoproject.eu/sites/default/files/pangeo_other/D3.5-PanGeo-Production-Manualv1.3pdf>, (accessed 07.03.14.).
Berti, M., Corsini, A., Franceschini, S., Jannacone, J.P., 2013. Automated classification of Persistent Scatterers Interferometry time series. Nat. Hazards Earth Syst. Sci. 13, 1945–1958.
Chang, L., Hanssen, R.F., 2014. Detection of cavity migration and sinkhole risk using radar interferometric time series. Remote Sens. Environ. 147 (5), 56–64.
Cigna, F., Bianchini, S., Casagli, N., 2013. How to assess landslide activity and intensity with Persistent Scatterer Interferometry (PSI): the PSI-based matrix approach. Landslides 10 (3), 267–283.
Cigna, F., Bateson, L.B., Jordan, C.J., Dashwood, C., 2014. Simulating SAR geometric distortions and predicting Persistent Scatterer densities for ERS-1/2 and ENVISAT C-band SAR and InSAR applications: nationwide feasibility assessment to monitor the landmass of Great Britain with SAR imagery. Remote Sens. Environ. 152, 441–466.
Colesanti, C., Wasowski, J., 2006. Investigating landslides with space-borne Synthetic Aperture Radar (SAR) interferometry. Eng. Geol. 88 (3–4), 173–199.
Crosetto, M., Monserrat, O., Iglesias, R., Crippa, B., 2010. Persistent scatterer interferometry: potential, limits and initial C- and X-band comparison. Photogramm. Eng. Remote Sens. 76 (9), 1061–1069.
Florence City Council, 2010. Piano Strutturale. Available at: </http://pianostrutturale.comune.fi.it/>.
Giannico, C., Ferretti, A., Alberti, S., Jurina, L., Ricci, M., Sciotti, A., 2013. Application of satellite radar interferometry for structural damage assessment and monitoring, In: Strauss, A., Frangopol, D., Bergmeiste K.,(Eds.), Life-Cycle and Sustainability of Civil Infrastructure.
Hanssen, R.F., 2005. Satellite radar interferometry for deformation monitoring: a priori assessment of feasibility and accuracy. Int. J. Appl. Earth Obs. 6, 253–260.
Nurul Wahida, R., Milton, G., Hamadan, N., Mohd. Iezuan Bin Nik Lah, N., Hakim Mohammed, A., 2012. Building condition assessment imperative and process. Procedia-Social Behav. Sci. 65, 775–780.
Osmanoğlu, B., Dixon, H.T., Wdowinski, S., Cabral-Cano, E., Jiang, Y., 2011. Mexico City subsidence observed with persistent scatterer InSAR. Int. J. Appl. Earth Obs. 13 (1), 1–12.
Salim, N.A.A., Zahari, N.F., 2011. Developing Integrated Building Indicator System (IBIS) a method of formulating the building condition rating. Procedia Eng. 20, 256–261.
Stramondo, S., Bozzano, F., Marra, F., Wegmuller, U., Cinti, F.R., Moro, M., Saroli, M., 2008. Subsidence induced by urbanisation in the city of Rome detected by advanced InSAR technique and geotechnical investigations. Remote Sens. Environ. 112, 3160–3172.
Tapete, D., Morelli, S., Fanti, R., Casagli, N., 2015. Localising deformation along the elevation of linear structures: an experiment with space-borne InSAR and RTK GPS on the Roman Aqueducts in Rome Italy. Appl. Geogr. 58, 65–83, http://dx.doi.org/10.1016/j.apgeog.2015.01.009.